J. Math. Computer Sci., 36 (2025), 142–162

Online: ISSN 2008-949X

Journal of Mathematics and Computer Science

Journal Homepage: www.isr-publications.com/jmcs

Exploring COVID-19 model with general fractional derivatives: novel Physics-Informed-Neural-Networks approach for dynamics and order estimation

Hassan Aghdaoui[a], Aeshah A. Raezah[b], Mouhcine Tilioua[a], Yassine Sabbar[a,*]

[a]MAIS Laboratory, MAMCS Group, FST Errachidia, Moulay Ismail University of Meknes, P.O. Box 509, Errachidia 52000, Morocco.

[b]Department of Mathematics, Faculty of Science, King Khalid University, Abha 62529, Saudi Arabia.

Abstract

In this paper, a fractional coronavirus disease model including unreported cases is suggested. The considered model includes a general fractional derivative incorporating well-known types, specifically Caputo-Fabrizio, Atangana-Baleanu and Weighted Atangana-Baleanu. Our theoretical results are two-fold. First, under suitable assumptions, the existence of a solution for the considered system is proven. Moreover, the local stability of the free-disease and endemic equilibrium points is addressed in terms of R_0. Secondly, a particular example is considered where the fractional derivative has two varying parameters, and an approach allowing for their estimation is proposed, with the aim of providing the best approximation of the real COVID-19 dynamics. The main novelty of our proposed approach is its use of physics-informed-neural-networks (PINNs) for estimating the fractional orders. On the other hand, to validate our results, a numerical simulations are conducted to illustrate the local stability of the disease dynamics, as well as the effectiveness of our proposed method in providing the best approximation of the two fractional derivative parameters.

Keywords: Epidemic model, incidence rate, equilibrium points, optimal control, numerical analysis.

2020 MSC: 92B05, 93D20.

1. Introduction

The COVID-19 outbreak has had a profound impact on global health. The virus, which emerged in 2019, quickly spread over a large region area. Drawing on prior experiences with outbreaks such as HIV, Zika, Ebola, cholera, and the Spanish flu, scientists and epidemiologists have assisted governments in swiftly implementing control measures. These measures include closing borders, enforcing lockdowns, isolating infected individuals, and sanitizing contaminated surfaces to manage this unprecedented crisis that affects public health, the economy, and society. Several advanced technologies are being used to expedite the mitigation process, including artificial intelligence-based algorithms for classifying infected

*Corresponding author
Email address: y.sabbar@umi.ac.ma (Yassine Sabbar)

doi: 10.22436/jmcs.036.02.01

Received: 2024-03-19 *Revised:* 2024-05-09 *Accepted:* 2024-05-27

cases, mathematical models to analyze disease spread dynamics [24], and Big-Data approaches for tracking population migration and identifying transmission hotspots [13]. Healthcare delivery encompasses emerging technologies to combat and anticipate emerging diseases. The main applications of artificial intelligence in the coronavirus pandemic include early identification and diagnosis of infections [17], treatment monitoring [8], forecasting of cases and deaths, tracing individuals' contacts, development of medicines and vaccines [31], reducing the responsibility of the healthcare professionals [15] and prevention of the diseases. Many mathematical models are employed to understand the progression of diseases, drawing from sources such as books and research on mathematical models in medicine and biology. The study [7] analyzes the dynamics of hepatitis B virus (HBV) epidemic using stochastic Lyapunov functional theory. In [16, 18] , the authors model the COVID-19 epidemic in various countries using early reported case data to project the cumulative number of reported cases over time. The model emphasizes the timing of key public policy measures that limit social movement, the identification and isolation of unreported cases, and the influence of asymptomatic infectious (refer to [1] for more information). Mathematicians have proposed so various types of non-integer order derivatives including Caputo, Caputo and Fabrizio, and Atangana-Baleanu. In [2], the authors organized a study of an epidemic model via Atangana-Baleanu fractional derivatives in Caputo sense and some results on existence and stability of solutions are established. Kumar et al. , addressed a coronavirus model with a time-delay in Caputo fractional derivatives using a predictor-corrector method. The concept of fractional derivative is an extension of the integer-order derivative. Recently, it has lately been utilized to investigate the influence of memory in dynamics systems from diverse disciplines such as virology, economics, ecology and epidemiology.

Machine learning approaches are highly successful in solving inverse problems and data-driven forward of the partial differential equations (PDEs). Neural networks, particularly physics-informed neural networks (PINNs), have a significant capacity for function approximation. The paper [20] employs advanced PINNs to estimate changing parameters in the SEIRD compartmental model. The results are compared with those of previous publications for analyzing COVID-19 transmission dynamics. In [36], the authors identify the distribution of parameters in stochastic PDEs and optimize complex systems using neural network algorithms as discussed in [29]. Various studies are performed in the field of fractional derivatives, incorporating neural networks and exploring different applications. In [11], the use of artificial neural networks (ANNs) for analyzing fractional differential equations in the Caputo sense is examined. This approach is extended to address higher-order fractional differential equations in [27]. In [22], researchers employ training ANN and optimization techniques to solve fractional differential equations, while the authors in [34] use wavelet neural networks to solve them. The authors in [30] present a numerical technique based on neural networks for generalized Caputo-type fractional differential equations. In [23, 37], a novel neural network scheme named fractional PINNs is discussed. The authors propose an adaptive loss weighting auxiliary output approach based on fractional physics-informed neural networks (fPINNs) to solve fractional partial integro-differential equations. The method effectively combines the automatic differentiation technique with a numerical differentiation algorithm to construct a universal numerical scheme for fractional derivatives of different orders.

The fundamental aspects of our model revolve around specific elements. Firstly, it focuses on the precise timing of implementating significant public policies to limit social mobility, secondly, it emphasizes the diligent identification and isolation of cases that have not been officially reported. Thirdly, it assesses the influence of asymptomatic infectious individuals. To achive this assessment, we employ a general fractional operator, including the Caputo-Fabrizio operator, which is useful for time-dependent problems, the Atangana-Baleanu operator, which has gained considerable interest in recent years, and the modified Atangana-Baleanu operator. We analyze the applicability and effects of these operators on the model and use a PINNs-based approach to estimate the fractional orders. The current study encompasses critical components of COVID-19 outbreaks, including the population of asymptomatic individuals exhibiting negligible symptoms, the cohort of symptomatic patients displaying severe symptoms who have been officially reported, and the group of symptomatic individuals with mild symptoms who remain unreported. Our primary objective is to advocate for incorporation general fractional derivatives into a

COVID-19 epidemic model and rigorously establish the specific conditions governing the existence and uniqueness of their solutions using a fixed point theory. Subsequently, we will elucidate the impact of these fractional derivatives, supported by artificial intelligence, through numerical simulations. Additionally, we will explore the aspects of hereditary properties and memory in fractional-order models.

The paper structure is presented as follows. In Section 2, we formulate the mathematical model for the COVID-19 disease and establish the number $\mathcal{R}_0$, as well as the stability of the disease-free and the endemic equilibrium points. In Section 3, we present numerical simulations to explain the results. In Section 4, we begin with a brief summary of the basics of machine learning and emphasize the importance of neural networks. Then, we explore the fundamentals of various neural network algorithms and techniques. Finally, we provide a brief discussion and conclusion in Section 5.

2. Preliminary results and description of the model

2.1. Preliminaries

We briefly provide some basic definitions and properties which will be useful in the next sections. We define the Banach space $\Omega = E \times E \times \cdots \times E$ and $E = C[0, T]$, with the norm

$$\|W\| = \|(w_1, w_2, \ldots, w_n)\| = \max_{t\in[0,T]} \{| w_1(t) | + | w_2(t) | + \cdots + | w_n(t) |\},$$

$w_i \in C[0, T]$ for $i = 1, \ldots, n$.

Definition 2.1 ([14]). We assume that $\alpha \in [0, 1)$ and β, γ are a positive parameters and $f \in H^1(a, b)$. The general fractional derivative of the function f in Caputo sens is defined as follows:

$$^{C}D^{\alpha,\beta,\gamma}_{a,t,w} f(t) = \frac{N(\alpha)}{1-\alpha}\frac{1}{w(t)}\int_a^t E_\beta[-\frac{\alpha}{1-\alpha}(t-z)^\gamma]\frac{d}{dz}(wf)(z)dz, \tag{2.1}$$

where E_β is a Mittag-Leffler function parametrized by β. N is a normalization function following $N(0) = N(1) = 1$ and w is a wieght function obeying $w > 0$ and $w' > 0$.

Definition 2.2 ([14]). Let $\alpha \in [0, 1)$ and β, γ are a positive parameters and $f \in H^1(a, b)$. The general fractional derivative of the function f of Riemann-Liouville sens is defined as follows:

$$^{R}D^{\alpha,\beta,\gamma}_{a,t,w} f(t) = \frac{N(\alpha)}{1-\alpha}\frac{1}{w(t)}\frac{d}{dt}\int_a^t E_\beta[-\frac{\alpha}{1-\alpha}(t-z)^\gamma]w(z)f(z)dz.$$

Theorem 2.3.

1. *Let wf be an analytic function, then:*

$$^{R}D^{\alpha,\beta,\gamma}_{a,t,w} f(t) = {}^{C}D^{\alpha,\beta,\gamma}_{a,t,w} f(t) + \frac{N(\alpha)}{1-\alpha}\frac{1}{w(t)}E_\beta[-\frac{\alpha}{1-\alpha}(t-a)^\gamma](wf)(a).$$

2. *When $w = 1, \beta = \gamma = 1$, we get the Caputo-Fabrizio fractional derivative.*
3. *When $w = 1, \alpha = \beta = \gamma$, we obtain the Atangana-Baleanu fractional derivative.*
4. *When $\alpha = \beta = \gamma$ we attain the weighted Atangana-Baleanu fractional derivative.*

Proof. Refer to [14]. □

Definition 2.4. When $\beta = \gamma$, the integral corresponding the general fractional derivative is defined as

$$I^{\alpha,\beta}_{a,t,w} f(t) = \frac{1-\alpha}{N(\alpha)}f(t) + \frac{\alpha}{\Gamma(\beta)N(\alpha)}\frac{1}{w(t)}\int_a^t (t-z)^{\beta-1}w(z)f(z)dz.$$

Theorem 2.5. *We consider $\Pi : F \longrightarrow F$ be a contraction mapping, where F is a Banach space. In this case, Π has a unique fixed point.*

2.2. The proposed model

We consider the epidemic model based on the differential equations introduced by Magal et al. in [16, 18]:

$$\begin{cases} \dfrac{dS(t)}{dt} = \Lambda - \tau(t)S(t)[I(t) + U(t)] - \mu S(t), \\ \dfrac{dI(t)}{dt} = \tau(t)S(t)[I(t) + U(t)] - (\nu + \mu)I(t), \\ \dfrac{dR(t)}{dt} = \nu_1 I(t) - (\eta + \mu)R(t), \\ \dfrac{dU(t)}{dt} = \nu_2 I(t) - (\eta + \mu)U(t), \\ \dfrac{dH(t)}{dt} = \eta(R(t) + U(t)) - \mu H(t), \end{cases} \tag{2.2}$$

where S refers to the total number of individuals who are **s**usceptible, I stands for the asymptomatic **i**nfectious individuals, R represents the total number of **r**eported infectious individuals showing symptoms, U signifies the **u**nreported infectious individuals showing symptoms, H indicates the total number of **h**ealed individuals, and τ is the transmission rate provided as follows:

$$\begin{cases} \tau(t) = \tau_0, & \text{for } t \in [0, N], \\ \tau(t) = \tau_0 e^{(-\mu_1(t-N))}, & N < t. \end{cases}$$

The parameters are defined as follows. Λ represents the flux of population, μ stands for the natural death rate, μ_1 denotes to the intensity of the public interventions, ν_1 indicates the transmission rate from I to R, ν_2 is the transmission rate from I to U and η signifies the transmission rate from the symptomatic individuals to H. The model supplemented by initial data $S_0 = S(t_0)$, $I_0 = I(t_0)$, $R_0 = R(t_0)$, $U_0 = U(t_0)$, and $H_0 = H(t_0)$. This model incorporates key features of the COVID-19 epidemic. First, it highlights the significance of the timing and magnitude of major government public restrictions designed to mitigate the severity of the epidemic. Secondly, it emphasizes the importance of both reported and unreported cases in interpreting the number of reported cases, and Lastly, it underscores the importance of asymptomatic infectious cases in disease transmission. In the model formulation, infectious individuals are divided into asymptomatic and symptomatic groups. Additionally, the symptomatic group is further classified into reported and unreported cases.

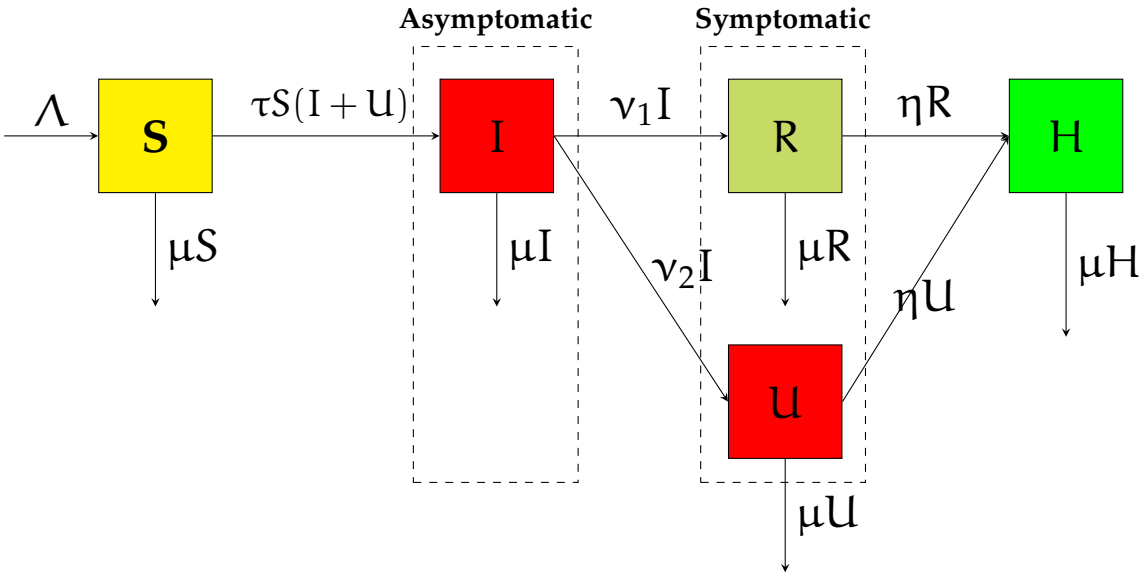

Figure 1: Illustrative diagram of the SIRUH model.

Now, we extend the previous model by substituting the integer-order derivative with the general fractional derivative, as follows:

$$\begin{cases} {}^{c}D^{\alpha,\beta,\gamma}_{a,t,w} S(t) = \Lambda - \tau(t)S(t)[I(t)+U(t)] - \mu S(t), \\ {}^{c}D^{\alpha,\beta,\gamma}_{a,t,w} I(t) = \tau(t)S(t)[I(t)+U(t)] - (\nu+\mu)I(t), \\ {}^{c}D^{\alpha,\beta,\gamma}_{a,t,w} R(t) = \nu_1 I(t) - (\eta+\mu)R(t), \\ {}^{c}D^{\alpha,\beta,\gamma}_{a,t,w} U(t) = \nu_2 I(t) - (\eta+\mu)U(t), \\ {}^{c}D^{\alpha,\beta,\gamma}_{a,t,w} H(t) = \eta(R(t)+U(t)) - \mu H(t). \end{cases} \tag{2.3}$$

2.3. Existence of solutions

We explore firstly, the existence of a solution for the epidemic simulation (2.3) using the fixed point technique. To this aim, we need to reformulate the model in the appropriate form:

$$\begin{cases} {}^{c}D^{\alpha,\beta,\gamma}_{a,t,w} S(t) = g_1(t,S), \\ {}^{c}D^{\alpha,\beta,\gamma}_{a,t,w} I(t) = g_2(t,I), \\ {}^{c}D^{\alpha,\beta,\gamma}_{a,t,w} R(t) = g_3(t,R), \\ {}^{c}D^{\alpha,\beta,\gamma}_{a,t,w} U(t) = g_4(t,U), \\ {}^{c}D^{\alpha,\beta,\gamma}_{a,t,w} H(t) = g_5(t,H), \end{cases}$$

where

$$\begin{cases} g_1(t,S) = \Lambda - \tau(t)S(t)[I(t)+U(t)] - \mu S(t), \\ g_2(t,I) = \tau(t)S(t)[I(t)+U(t)] - (\nu+\mu)I(t), \\ g_3(t,R) = \nu_1 I(t) - (\eta+\mu)R(t), \\ g_4(t,U) = \nu_2 I(t) - (\eta+\mu)U(t), \\ g_5(t,H) = \eta(R(t)+U(t)) - \mu H(t). \end{cases}$$

The fractional integral equation when $\beta = \gamma$ is as follows:

$$\begin{cases} S(t) - S(0) = \frac{1-\alpha}{N(\alpha)} g_1(t,S) + \frac{\alpha}{\Gamma(\beta)N(\alpha)w(t)} \int_0^t g_1(z,S) w(z)(t-z)^{\beta-1} dz, \\ I(t) - I(0) = \frac{1-\alpha}{N(\alpha)} g_2(t,I) + \frac{\alpha}{\Gamma(\beta)N(\alpha)w(t)} \int_0^t g_2(z,I) w(z)(t-z)^{\beta-1} dz, \\ R(t) - R(0) = \frac{1-\alpha}{N(\alpha)} g_3(t,R) + \frac{\alpha}{\Gamma(\beta)N(\alpha)w(t)} \int_0^t g_3(z,R) w(z)(t-z)^{\beta-1} dz, \\ U(t) - U(0) = \frac{1-\alpha}{N(\alpha)} g_4(t,U) + \frac{\alpha}{\Gamma(\beta)N(\alpha)w(t)} \int_0^t g_4(z,U) w(z)(t-z)^{\beta-1} dz, \\ H(t) - H(0) = \frac{1-\alpha}{N(\alpha)} g_5(t,H) + \frac{\alpha}{\Gamma(\beta)N(\alpha)w(t)} \int_0^t g_5(z,H) w(z)(t-z)^{\beta-1} dz. \end{cases}$$

Theorem 2.6. *For each* $i \in \{1,\dots,5\}$, *the kernels* g_i $(i = 1,\dots,5)$ *are* L_i*-Lipschitz continuous. Furthermore, if* $L_i < 1$, $\forall i \in \{1,\dots,5\}$, *then the kernels define a contraction in* $C(0,T)$.

Proof. Let $S, I, R, U, H, \tau \in C[0,T]$, and consider:

$$\|S\| \leqslant a, \quad \|I\| \leqslant b, \quad \|R\| \leqslant c, \quad \|U\| \leqslant d, \quad \|H\| \leqslant e, \quad \|\tau\| \leqslant f.$$

Let S and S^* be given, then it holds that

$$\begin{aligned} \|g_1(t,S) - g_1(t,S^*)\| &= \|\Lambda - \tau(t)S(t)[I(t)+U(t)] - \mu S(t) - (\Lambda - \tau(t)S^*(t)[I(t)+U(t)] - \mu S^*(t))\| \\ &= \| (\tau(t)(I(t)+U(t)) + \mu)(S^*(t) - S(t)) \| \\ &\leqslant \|\tau(t)(I(t)+U(t)) + \mu\| \|S^*(t) - S(t)\| \end{aligned}$$

$$\begin{aligned}&\leqslant [\|\tau(t)\| (\|I(t)\| + \|U(t)\|) + \mu] \|S^*(t) - S(t)\| \\ &\leqslant [f(b+d) + \mu] \|S^*(t) - S(t)\|.\end{aligned}$$

Consequently,

$$\|g_1(t,S) - g_1(t,S^*)\| \leqslant L_1 \|S(t) - S^*(t)\|,$$

where $L_1 = f(b+d) + \mu$. Obviously, the Lipschitz condition is verified for g_1. Moreover, if $0 \leqslant L_1 < 1$, then g_1 defined a contraction. Likewise, we can show that g_2, g_3, g_4, and g_5 satisfy the contraction and Lipschitz properties. Therefore,

$$\begin{cases} \|g_2(t,I) - g_2(t,I^*)\| \leqslant L_2 \|I(t) - I^*(t)\|, \\ \|g_3(t,R) - g_3(t,R^*)\| \leqslant L_3 \|R(t) - R^*(t)\|, \\ \|g_4(t,U) - g_4(t,U^*)\| \leqslant L_4 \|U(t) - U^*(t)\|, \\ \|g_5(t,H) - g_5(t,H^*)\| \leqslant L_5 \|H(t) - H^*(t)\|, \end{cases}$$

where

$$L_2 = f\alpha + \nu + \mu, \quad L_3 = L_4 = \eta + \mu, \quad L_5 = \mu.$$

□

Theorem 2.7. *If*

$$\left[\frac{1-\alpha}{N(\alpha)} + \frac{\alpha w(T) T^\beta}{\beta \Gamma(\beta) N(\alpha)} \left\|\frac{1}{w}\right\|\right] L_i < 1, \quad i \in \{1, 2, \ldots, 5\},$$

the fractional model has unique solution.

Proof. Given the initial data

$$S(0) = S_0(t), \quad I(0) = I_0(t), \quad U_0(t) = U(0), \quad R(0) = R_0(t), \quad H_0(t) = H(0),$$

we analyze the iterative sequence:

$$\begin{cases} S_n(t) = S_0(t) + \frac{1-\alpha}{N(\alpha)} g_1(t, S_{n-1}) + \frac{\alpha}{\Gamma(\beta) N(\alpha) w(t)} \int_0^t g_1(z, S_{n-1}) w(z) (t-z)^{\beta-1} dz, \\ I_n(t) = I_0(t) + \frac{1-\alpha}{N(\alpha)} g_2(t, I_{n-1}) + \frac{\alpha}{\Gamma(\beta) N(\alpha) w(t)} \int_0^t g_2(z, I_{n-1}) w(z) (t-z)^{\beta-1} dz, \\ R_n(t) = R_0(t) + \frac{1-\alpha}{N(\alpha)} g_3(t, R_{n-1}) + \frac{\alpha}{\Gamma(\beta) N(\alpha) w(t)} \int_0^t g_3(z, R_{n-1}) w(z) (t-z)^{\beta-1} dz, \\ U_n(t) = U_0(t) + \frac{1-\alpha}{N(\alpha)} g_4(t, U_{n-1}) + \frac{\alpha}{\Gamma(\beta) N(\alpha) w(t)} \int_0^t g_4(z, U_{n-1}) w(z) (t-z)^{\beta-1} dz, \\ H_n(t) = H_0(t) + \frac{1-\alpha}{N(\alpha)} g_5(t, H_{n-1}) + \frac{\alpha}{\Gamma(\beta) N(\alpha) w(t)} \int_0^t g_5(z, H_{n-1}) w(z) (t-z)^{\beta-1} dz. \end{cases}$$

The successive difference between the terms leads to:

$$\begin{cases} \Phi_{1n}(t) = S_n(t) - S_{n-1}(t) = \frac{1-\alpha}{N(\alpha)}\left[g_1(t, S_{n-1}) - g_1(t, S_{n-2})\right] \\ \qquad + \frac{\alpha}{N(\alpha)\Gamma(\beta)}\frac{1}{w(t)}\int_0^t \left[g_1(z, S_{n-1}) - g_1(z, S_{n-2})\right] w(z)(t-z)^{\beta-1}dz, \\ \Phi_{2n}(t) = I_n(t) - I_{n-1}(t) = \frac{1-\alpha}{N(\alpha)}\left[g_2(t, I_{n-1}) - g_2(t, I_{n-2})\right] \\ \qquad + \frac{\alpha}{N(\alpha)\Gamma(\beta)}\frac{1}{w(t)}\int_0^t \left[g_2(z, I_{n-1}) - g_2(z, I_{n-2})\right] w(z)(t-z)^{\beta-1}dz, \\ \Phi_{3n}(t) = R_n(t) - R_{n-1}(t) = \frac{1-\alpha}{N(\alpha)}\left[g_3(t, R_{n-1}) - g_3(t, R_{n-2})\right] \\ \qquad + \frac{\alpha}{N(\alpha)\Gamma(\beta)}\frac{1}{w(t)}\int_0^t \left[g_3(z, R_{n-1}) - g_3(z, R_{n-2})\right] w(z)(t-z)^{\beta-1}dz, \\ \Phi_{4n}(t) = U_n(t) - U_{n-1}(t) = \frac{1-\alpha}{N(\alpha)}\left[g_4(t, U_{n-1}) - g_4(t, U_{n-2})\right] \\ \qquad + \frac{\alpha}{N(\alpha)\Gamma(\beta)}\frac{1}{w(t)}\int_0^t \left[g_4(z, U_{n-1}) - g_4(z, U_{n-2})\right] w(z)(t-z)^{\beta-1}dz, \\ \Phi_{5n}(t) = H_n(t) - H_{(n-1)}(t) = \frac{1-\alpha}{N(\alpha)}\left[g_5\left(t, H_{(n-1)}\right) - g_5\left(t, H_{(n-2)}\right)\right] \\ \qquad + \frac{\alpha}{N(\alpha)\Gamma(\beta)}\frac{1}{w(t)}\int_0^t \left[g_5\left(z, H_{(n-1)}\right) - g_5\left(z, H_{(n-2)}\right)\right] w(z)(t-z)^{\beta-1}dz. \end{cases}$$

Clearly, we have

$$S_n(t) - S_0(t) = \sum_{l=1}^{n} \Phi_{1l}(t) = \sum_{l=1}^{n} (S_l(t) - S_{l-1}), \qquad I_n(t) - I_0(t) = \sum_{l=1}^{n} \Phi_{2l}(t), \quad R_n(t) - R_0(t) = \sum_{l=1}^{n} \Phi_{3l}(t),$$

$$U_n(t) - U_0(t) = \sum_{l=1}^{n} \Phi_{4l}(t), \qquad H_n(t) - H_0(t) = \sum_{l=1}^{n} \Phi_{5l}(t).$$

By taking the norm of equations, we obtain

$$\begin{cases} \|\Phi_{1n}(t)\| \leqslant \frac{1-\alpha}{N(\alpha)} L_1 \|\Phi_{1(n-1)}(t)\| + \frac{\alpha}{N(\alpha)\Gamma(\beta)} \|\frac{1}{w}\| L_1 \int_0^t \|\Phi_{1(n-1)}(z)\| w(z)(t-z)^{\beta-1}dz, \\ \|\Phi_{2n}(t)\| \leqslant \frac{1-\alpha}{N(\alpha)} L_2 \|\Phi_{2(n-1)}(t)\| + \frac{\alpha}{N(\alpha)\Gamma(\beta)} \|\frac{1}{w}\| L_2 \int_0^t \|\Phi_{2(n-1)}(z)\| w(z)(t-z)^{\beta-1}dz, \\ \|\Phi_{3n}(t)\| \leqslant \frac{1-\alpha}{N(\alpha)} L_3 \|\Phi_{3(n-1)}(t)\| + \frac{\alpha}{N(\alpha)\Gamma(\beta)} \|\frac{1}{w}\| L_3 \int_0^t \|\Phi_{3(n-1)}(z)\| w(z)(t-z)^{\beta-1}dz, \\ \|\Phi_{4n}(t)\| \leqslant \frac{1-\alpha}{N(\alpha)} L_4 \|\Phi_{4(n-1)}(t)\| + \frac{\alpha}{N(\alpha)\Gamma(\beta)} \|\frac{1}{w}\| L_4 \int_0^t \|\Phi_{4(n-1)}(z)\| w(z)(t-z)^{\beta-1}dz, \\ \|\Phi_{5n}(t)\| \leqslant \frac{1-\alpha}{N(\alpha)} L_5 \|\Phi_{5(n-1)}(t)\| + \frac{\alpha}{N(\alpha)\Gamma(\beta)} \|\frac{1}{w}\| L_5 \int_0^t \|\Phi_{5(n-1)}(z)\| w(z)(t-z)^{\beta-1}dz. \end{cases}$$

Since $w \in C^1[0, T]$, $w > 0$, $w' > 0$, then $w(t) \leqslant w(T)$, $\forall t \in [0, T]$. Consequently,

$$\begin{cases} \|\Phi_{1n}(t)\| \leqslant \|\Phi_{1(n-1)}(t)\| \left[\frac{1-\alpha}{N(\alpha)} L_1 + \frac{\alpha w(T) T^{\beta}}{\beta N(\alpha)\Gamma(\beta)} \|\frac{1}{w}\| L_1\right], \\ \|\Phi_{2n}(t)\| \leqslant \|\Phi_{2(n-1)}(t)\| \left[\frac{1-\alpha}{N(\alpha)} L_2 + \frac{\alpha w(T) T^{\beta}}{\beta N(\alpha)\Gamma(\beta)} \|\frac{1}{w}\| L_2\right], \\ \|\Phi_{3n}(t)\| \leqslant \|\Phi_{3(n-1)}(t)\| \left[\frac{1-\alpha}{N(\alpha)} L_3 + \frac{\alpha w(T) T^{\beta}}{\beta N(\alpha)\Gamma(\beta)} \|\frac{1}{w}\| L_3\right], \\ \|\Phi_{4n}(t)\| \leqslant \|\Phi_{4(n-1)}(t)\| \left[\frac{1-\alpha}{N(\alpha)} L_4 + \frac{\alpha w(T) T^{\beta}}{\beta N(\alpha)\Gamma(\beta)} \|\frac{1}{w}\| L_4\right], \\ \|\Phi_{5n}(t)\| \leqslant \|\Phi_{5(n-1)}(t)\| \left[\frac{1-\alpha}{N(\alpha)} L_5 + \frac{\alpha w(T) T^{\beta}}{\beta N(\alpha)\Gamma(\beta)} \|\frac{1}{w}\| L_5\right]. \end{cases}$$

Thereby,

$$\begin{cases} \|\Phi_{1n}(t)\| \leqslant \|S_1(t)-S_0(t)\| \left[\dfrac{1-\alpha}{N(\alpha)}L_1+\dfrac{\alpha w(T)T^{\beta}}{\beta N(\alpha)\Gamma(\beta)}\|\frac{1}{w}\|L_1\right]^{n-1}, \\ \|\Phi_{2n}(t)\| \leqslant \|I_1(t)-I_0(t)\| \left[\dfrac{1-\alpha}{N(\alpha)}L_2+\dfrac{\alpha w(T)T^{\beta}}{\beta N(\alpha)\Gamma(\beta)}\|\frac{1}{w}\|L_2\right]^{n-1}, \\ \|\Phi_{3n}(t)\| \leqslant \|R_1(t)-R_0(t)\| \left[\dfrac{1-\alpha}{N(\alpha)}L_3+\dfrac{\alpha w(T)T^{\beta}}{\beta N(\alpha)\Gamma(\beta)}\|\frac{1}{w}\|L_3\right]^{n-1}, \\ \|\Phi_{4n}(t)\| \leqslant \|U_1(t)-U_0(t)\| \left[\dfrac{1-\alpha}{N(\alpha)}L_4+\dfrac{\alpha w(T)T^{\beta}}{\beta N(\alpha)\Gamma(\beta)}\|\frac{1}{w}\|L_4\right]^{n-1}, \\ \|\Phi_{5n}(t)\| \leqslant \|H_1(t)-H_0(t)\| \left[\dfrac{1-\alpha}{N(\alpha)}L_5+\dfrac{\alpha w(T)T^{\beta}}{\beta N(\alpha)\Gamma(\beta)}\|\frac{1}{w}\|L_5\right]^{n-1}. \end{cases}$$

Thus, the existence and continuity of the aforementioned solutions have been established. Now, our goal is to show that the above functions are solutions of (2.3). Assuming that:

$$S(t)-S(0)=S_n(t)-K_n(t), \quad I(t)-I(0)=I_n(t)-l_n(t), \quad R(t)-R(0)=R_n(t)-V_n(t),$$
$$U(t)-U(0)=U_n(t)-O_n(t), \quad H(t)-H(0)=H_n(t)-P_n(t).$$

Next, we have

$$\begin{aligned} \|K_n(t)\| &= \left\| \frac{1-\alpha}{N(\alpha)}\left[g_1(t,S)-g_1(t,S_{n-1})\right]+\frac{\alpha}{\Gamma(\beta)N(\alpha)w(t)}\int_0^t (t-z)^{\beta-1}\left[g_1(z,S)-g_1(z,S_{n-1})w(z)\right]dz \right\| \\ &\leqslant \frac{1-\alpha}{N(\alpha)}\|g_1(t,S)-g_1(t,S_{n-1})\|+\frac{\alpha}{\Gamma(\beta)N(\alpha)}\|\frac{1}{w}\|\int_0^t (t-z)^{\beta-1}w(z)\|g_1(z,S)-g_1(z,S_{n-1})\,dz\| \\ &\leqslant \frac{1-\alpha}{N(\alpha)}L_1\|S-S_{n-1}\|+\frac{\alpha w(T)T^{\beta}}{\beta N(\alpha)\Gamma(\beta)}\|\frac{1}{w}\|L1\|S-S_{n-1}\|. \end{aligned}$$

By continuing this method recursively, we obtain at time T:

$$\|K_n(t)\| \leqslant \left(\frac{1-\alpha}{N(\alpha)}+\frac{\alpha w(T)T^{\beta}}{\beta N(\alpha)\Gamma(\beta)}\|\frac{1}{w}\|\right)^{n+1} L_1^{n+1}a.$$

As n approaches infinity, we find that $\|K_n(t)\| \to 0$. Similarly, it can be observed that, $\|l_n(t)\|$, $\|V_n(t)\|$, $\|O_n(t)\|$, and $\|P_n(t)\|$ also tend towards zero. It is another crucial subject to demonstrate the uniqueness of the solutions of (2.3). Let $S_1(t)$, $I_1(t)$, $R_1(t)$, $U_1(t)$, and $H_1(t)$ be another solutions of the model (2.3), we find:

$$S(t)-S_1(t)=\frac{1-\alpha}{N(\beta)}\left[g_1(t,S)-g_1(t,S_1)\right]+\frac{\alpha}{\Gamma(\beta)N(\alpha)w(t)}\int_0^t (t-z)^{\beta-1}w(z)\left[g_1(z,S)-g_1(z,S_1)\right]dz.$$

Taking the norm, and considering that the kernel satisfies the Lipschitz condition, we obtain:

$$\|S(t)-S_1(t)\| \leqslant \frac{1-\alpha}{N(\alpha)}L_1\|S(t)-S_1(t)\|+\frac{\alpha w(T)T^{\beta}}{\beta\Gamma(\alpha)N(\alpha)}\|\frac{1}{w}\|L_1\|S(t)-S_1(t)\|.$$

This leads to the following inequality:

$$\|S(t)-S_1(t)\|\left(1-\frac{1-\alpha}{N(\alpha)}L_1-\frac{\alpha w(T)T^{\beta}}{\beta N(\alpha)\Gamma(\beta)}\|\frac{1}{w}\|L_1\right) \leqslant 0.$$

If the following inequality is satisfied:

$$\left(1-\frac{1-\alpha}{N(\alpha)}L_1-\frac{\alpha w(T)T^{\beta}}{\beta\Gamma(\beta)N(\alpha)}\|\frac{1}{w}\|L_1\right)>0,$$

then, $\|S(t)-S_1(t)\|=0$. Therefore, we have $S(t)=S_1(t)$. With the same method, we can get the unique solution for I, R, U, and H. Consequently, the solution is unique. This completes the proof.

□

2.4. Stability results

In this section, we examine the stability of the model (2.3). First, we calculate the endemic equilibrium and the basic reproduction number $\mathcal{R}_0$. Then, we present the stability results.

2.4.1. Basic reproduction number $\mathcal{R}_0$

The disease-free equilibrium state is achieved by making $I=0$:

$$X_0=(\frac{\Lambda}{\mu},0,0,0).$$

The infectious part of the system is expressed as:

$$\begin{cases}\dfrac{dI(t)}{dt}=\tau(t)S(t)[I(t)+U(t)]-(\nu+\mu)I(t),\\ \dfrac{dU(t)}{dt}=\nu_2 I(t)-(\eta+\mu)U(t).\end{cases}$$

The corresponding matrix is:

$$A=\begin{pmatrix}\tau_0S^0-(\nu+\mu) & \tau_0S^0\\ \nu_2 & -(\eta+\mu)\end{pmatrix}=V-S,$$

where

$$V=\begin{pmatrix}\tau_0S^0 & \tau_0S^0\\ \nu_2 & 0\end{pmatrix},\quad S=\begin{pmatrix}\nu+\mu & 0\\ 0 & \eta+\mu\end{pmatrix},\quad \text{and}\quad S^0=\frac{\Lambda}{\mu}.$$

The next-generation matrix (NGM) [6] is:

$$VS^{-1}=\begin{pmatrix}\dfrac{\tau_0S^0}{\nu+\mu} & \dfrac{\tau_0S^0}{\eta+\mu}\\ \dfrac{\nu_2}{\nu+\mu} & 0\end{pmatrix}.$$

Therefore,

$$\mathcal{R}_0=\frac{\nu_2\tau_0S^0}{(\nu+\mu)(\eta+\mu)}.$$

2.4.2. Endemic equilibrium state

The system (2.3) admits a unique endemic equilibrium determined by setting the right-hand side to zero, $X^*=(S^*,I^*,R^*,U^*,H^*)$ such that

$$S^*=\frac{(\eta+\mu)(\nu+\mu)}{\tau_0[\eta+\mu+\nu_2]},\quad I^*=\frac{\Lambda}{\nu+\mu}-\frac{\mu(\eta+\mu)}{\tau_0[\eta+\mu+\nu_2]},\quad R^*=\frac{\nu_1}{\eta+\mu}I^*,\quad U^*=\frac{\nu_2}{\eta+\mu}I^*,\quad H^*=\frac{\eta\nu}{\mu(\eta+\mu)}I^*.$$

Theorem 2.8.

- *If $\mathcal{R}_0<\dfrac{\nu_2}{\nu_2+\eta+\mu}$ ($\mathcal{R}_0<1$), then the disease-free equilibrium point X_0 is locally asymptotically stable.*

- *On the other hand, if* $\mathcal{R}_0 > \dfrac{\nu_2}{\nu_2+\eta+\mu}$ *(*$\mathcal{R}_0 > 1$*), then the endemic equilibrium point* X^* *is locally asymptotically stable.*

Proof.

Local stability of X_0: By linearizing the system (2.3) at X_0, the Jacobian matrix is given by:

$$J(X_0) = \begin{pmatrix} -\mu & -\tau_0 S^0 & 0 & -\tau_0 S^0 & 0 \\ 0 & \tau_0 S^0 - (\nu+\mu) & 0 & \tau_0 S^0 & 0 \\ 0 & \nu_1 & -(\eta+\mu) & 0 & 0 \\ 0 & \nu_2 & 0 & -(\eta+\mu) & 0 \\ 0 & 0 & \eta & \eta & -\mu \end{pmatrix}.$$

The characteristic equation associated is:

$$P(X) = (X+\mu)^2(X+\eta+\mu)\big(X^2 + (\nu+\eta+2\mu-\tau_0 S^0)X - (\tau_0 S^0 - (\nu+\mu))(\eta+\mu) - \nu_2\tau_0 S^0\big).$$

The equation has real roots, which are given by:

$$\begin{aligned} X_1 &= -\mu < 0, \\ X_2 &= -(\eta+\mu) < 0, \\ X_3X_4 &= -(\tau_0 S^0 - (\nu+\mu))(\eta+\mu) - \nu_2\tau_0 S^0 = \frac{1}{\nu_2}(\nu_2+\eta+\mu)(\nu+\mu)(\eta+\mu)\Big(\frac{\nu_2}{\nu_2+\eta+\mu} - \mathcal{R}_0\Big) > 0, \\ X_3 + X_4 &= \tau_0 S^0 - (\nu+\eta+2\mu) \\ &= \frac{\nu_2}{(\nu+\mu)(\eta+\mu)}\Big(\mathcal{R}_0 - \nu_2\big(\frac{1}{\nu+\mu} + \frac{1}{\nu+\mu}\big)\Big) < 0 \quad \Big(\frac{\nu_2}{\nu_2+\eta+\mu} < \nu_2\big(\frac{1}{\nu+\mu} + \frac{1}{\nu+\mu}\big)\Big). \end{aligned}$$

Thus $|\arg(X_i)| = \pi > \dfrac{\alpha\pi}{2}$ for $i = 1,2,3,4$. Then, by applying the Routh-Hurwitz criterion, we have the local stability of X_0.

Local stability of X^*: The Jacobian matrix by linearizing the system (2.3) at X^* is:

$$J(X^*) = \begin{pmatrix} -\tau(I^*+U^*) - \mu & -\tau S^* & 0 & -\tau S^* & 0 \\ \tau(I^*+U^*) & \tau S^* - (\mu+\nu) & 0 & \tau S^* & 0 \\ 0 & \nu_1 & -(\eta+\mu) & 0 & 0 \\ 0 & \nu_2 & 0 & -(\eta+\mu) & 0 \\ 0 & 0 & \eta & \eta & -\mu \end{pmatrix}.$$

The characteristic equation is as

$$P(X) = (X+\mu)(\eta+\mu+X)\big(X^3 + a_1X^2 + a_2X + a_3\big),$$

where

$$\begin{aligned} a_1 &= \tau(I^*+U^*) + \nu + \eta + 3\mu + \tau S^*, \\ a_2 &= \tau(I^*+U^*)(\eta+\nu+2\mu) + (\eta+2\mu)(\nu+\mu) + (\eta+\mu)\mu - (\nu_2+\eta+2\mu)\tau S^* \\ &= \tau(I^*+U^*)(\eta+\nu+2\mu) + \mu(\nu+\mu) + (\eta+\mu)\mu\frac{\eta-\nu_1}{\eta+\nu_2+\mu}, \\ a_3 &= \tau(I^*+U^*)(\eta+\mu)(\mu+\nu) + (\eta+\mu)(\mu+\nu)\mu - (\nu_2\mu + (\mu+\eta)\mu)\tau S^* = \tau(I^*+U^*)(\eta+\mu)(\nu+\mu). \end{aligned}$$

Let

$$\begin{aligned} a_1a_2 - a_3 &= \big[\nu+\eta+3\mu+\tau S^*\big]a_2 + \tau(I^*+U^*)\big[\tau(I^*+U^*)(\eta+\nu+2\mu) \\ &\quad + \mu(\nu+\mu) + (\eta+\mu)\mu - (\nu_2+\eta+2\mu)\tau S^*\big] \\ &= \big[\nu+\eta+3\mu+\tau S^*\big]a_2 + \tau(I^*+U^*)\big[\tau(I^*+U^*)(\eta+\nu+2\mu) + \mu(\nu+\mu) + (\eta+\mu)\mu\frac{\eta-\nu_1}{\eta+\nu_2+\mu}. \end{aligned}$$

One can see that a_1, a_2, a_3, and $a_1a_2 - a_3$ are all positive. As a consequence of [4] and by applying Hurwitz's criterion, we have the local asymptotic stability of X^*. □

3. Numerical approach and discussion

3.1. Lagrange interpolation polynomial method

The numerical simulations are acquired by introducing an iterative method. To attain this, we used the Lagrange interpolation polynomial method to approximate fractional derivatives due to its high accuracy in approximating functions, smoothness, and adaptability in handling non-integer orders by adjusting the degree of the polynomial. This method makes an efficient approach for approximating fractional derivatives, ensuring smooth transitions and compatibility with PINNs, making it an effective choice for handling fractional derivatives in simulations. In a similar way to the modified fractional approach used in the paper [32], the fractional integral is approximated by employing the two-point Lagrange interpolation polynomial. So, for $t = t_{n+1}$, $n = 0, 1, \dots$ we obtain:

$$
\begin{aligned}
S(t_{n+1}) &= S(t_0) + \frac{1-\alpha}{N(\alpha)} g_1(t_n, S(t_n)) + \frac{\alpha}{\Gamma(\beta+2)N(\alpha)w(t)} \\
&\quad \times \sum_{p=0}^{n} \Big[h^{\alpha} g_1(t_n, S(t_p)) w(t_n) \left((n-p+1)^{\beta}(n-p+\beta+2) - (n-p)^{\beta}(n-p+2\beta+2) \right) \\
&\quad - h^{\beta} g_1(t_{p-1}, S(t_p)) w(t_{p-1}) \left((n-p+1)^{\beta+1} - (n-p)^{\beta}(n+1-p+\beta) \right) \Big], \\
I(t_{n+1}) &= I(t_0) + \frac{1-\alpha}{N(\alpha)} g_2(t_n, I(t_n)) + \frac{\alpha}{\Gamma(\beta+2)N(\alpha)w(t)} \\
&\quad \times \sum_{p=0}^{n} \Big[h^{\alpha} g_2(t_n, I(t_p)) w(t_n) \left((n-p+1)^{\beta}(n-p+\beta+2) - (n-p)^{\beta}(n-p+2\beta+2) \right) \\
&\quad - h^{\beta} g_2(t_{p-1}, I(t_p)) w(t_{p-1}) \left((n-p+1)^{\beta+1} - (n-p)^{\beta}(n+1-p+\beta) \right) \Big], \\
R(t_{n+1}) &= R(t_0) + \frac{1-\alpha}{N(\alpha)} g_3(t_n, R(t_n)) + \frac{\alpha}{\Gamma(\beta+2)N(\alpha)w(t)} \\
&\quad \times \sum_{p=0}^{n} \Big[h^{\alpha} g_3(t_n, R(t_p)) w(t_n) \left((n-p+1)^{\beta}(n-p+\beta+2) - (n-p)^{\beta}(n-p+2\beta+2) \right) \\
&\quad - h^{\beta} g_3(t_{p-1}, R(t_p)) w(t_{p-1}) \left((n-p+1)^{\beta+1} - (n-p)^{\beta}(n+1-p+\beta) \right) \Big], \\
U(t_{n+1}) &= U(t_0) + \frac{1-\alpha}{N(\alpha)} g_4(t_n, U(t_n)) + \frac{\alpha}{\Gamma(\beta+2)N(\alpha)w(t)} \\
&\quad \times \sum_{p=0}^{n} \Big[h^{\alpha} g_4(t_n, U(t_p)) w(t_n) \left((n-p+1)^{\beta}(n-p+\beta+2) - (n-p)^{\beta}(n-p+2\beta+2) \right) \\
&\quad - h^{\beta} g_4(t_{p-1}, U(t_p)) w(t_{p-1}) \left((n-p+1)^{\beta+1} - (n-p)^{\beta}(n+1-p+\beta) \right) \Big], \\
H(t_{n+1}) &= H(t_0) + \frac{1-\alpha}{N(\alpha)} g_5(t_n, H(t_n)) + \frac{\alpha}{\Gamma(\beta+2)N(\alpha)w(t)} \\
&\quad \times \sum_{p=0}^{n} \Big[h^{\alpha} g_5(t_n, H(t_p)) w(t_n) \left((n-p+1)^{\beta}(n-p+\beta+2) - (n-p)^{\beta}(n-p+2\beta+2) \right) \\
&\quad - h^{\beta} g_1(t_{p-1}, S(t_p)) w(t_{p-1}) \left((n-p+1)^{\beta+1} - (n-p)^{\beta}(n+1-p+\beta) \right) \Big].
\end{aligned}
$$

We consider the initial data: $S_0 = S(0) = 51.47 \times 10^6$, $I_0 = I(0) = 343$, $R_0 = R(0) = 379$, $U_0 = U(0) = 45$, $H(0) = H_0 = 5$, $\tau(t) = \tau_0$, and $w(t) = 1$ for the weighted Atangana-Baleanu. We conduct a numerical investigation into the influence of the generalized fractional derivative, involving the Caputo-Fabrizio (CF), the Atangana-Baleanu (AB), and Weighted Atangana-Baleanu (WAB) operators. Figure 2 illustrates the results obtained for different operators. For all parameter values, please refer to the Table 1. The

considered model contains five compartments, reflecting the current global situation. These types of models are valuable for examining the nature and predicting the exponential growth of the diseases. We deduce from the curves that each compartment's behavior is significantly influenced by the time and the considered fractional derivative. Furthermore, we observe behavior that corresponds to the parameters α, β, and γ. We note that the projected system simulates the behavior using the parameters listed in Table 1 and the fractional order. The observed behavior demonstrates the efficiency and performance of the considered solutions. From the figures, the proposed model strongly depends on the fractional order and provides a higher degree of adaptability. Moreover, the considered fractional operator presents more interesting results for examining and predicting the model in the future. This epidemic model depends into account hereditary properties, which aid in understanding and comprehending this mortal virus.

Table 1: Numerical values of the model parameters.

Parameter	Description	Value	Source
S_0	Initial susceptible population	51.47×10^6	Fitted
I_0	Initial infected population	343	Fitted
R_0	Initial reported population	379	Fitted
U_0	Initial unreported population	45	Fitted
H_0	Initial recovred population	5	Fitted
τ_0	Transmission rate	7.51×10^{-9}	[18]
μ	Natural death rate	0.001	Fitted
μ_1	Intensity of the public interventions	fixed	[16]
Λ	Flux of population	1000	Fitted
ν_1	Transmission rate from I to R	0.072	[18]
ν_2	Transmission rate from I to U	0.337	[18]
η	Transmission rate from the R or U to H	$\frac{1}{7}$	[18]

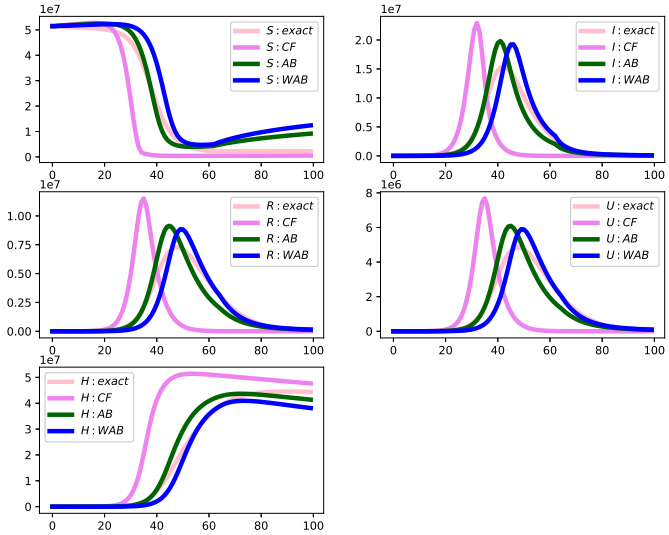

Figure 2: Solutions corresponding to different fractional derivatives: Caputo-Fabrizio (CF), Atangana-Baleanu (AB), and Weighted Atangana-Baleanu (WAB). The term "Exact" refers to the solution obtained using the odeint function from the scipy.integrate module in the Python scientific computing library, SciPy.

3.2. Sensitivity analysis

Sensitivity analysis plays a pivotal role in the fields of dynamic models study, particularly in areas like epidemiology and ecology [5, 19]. One fundamental element of this study involves examining the sensitivity of parameters, which entails calculating precise sensitivity measures for each parameter to understand their impact to disease dynamics. This section focuses on the sensitivity analysis of different parameters regarding R_0.

To conduct a sensitivity study, we compute the normalized forward sensitivity index for a parameter using the given formula:

$$SI_\sigma = \frac{\sigma}{R_0}\frac{\partial R_0}{\partial \sigma}, \tag{3.1}$$

This expression gives the sensitivity index of R_0 pertaining to the parameter σ. In the realm of forward sensitivity examination, we investigate how changes in these parameters affect the value of R_0. This investigative strategy enables us to evaluate the sensitivity of R_0 to enhancements in each parameter, providing profound understanding into their respective influences on the dynamic systems.

Using formula (3.1) to all parameters of the system (2.3), we observe the following outcomes.

(i) Parameters with positive sensitivity indices include Λ, τ_0, and ν_2, with:

$$SI_\Lambda = 1, \quad SI_{\tau_0} = 1, \quad SI_{\nu_2} = \frac{\nu_1 + \mu}{\nu_1 + \mu}.$$

This means that any modification in the values of these parameters directly impacts R_0, conducting to either a decrease or an increase in its value.

(ii) Parameters displaying a negative sensitivity measures, indicating that an increase in their values heads to a decrease in R_0, include μ, ν_1, and η, as detailed below:

$$SI_\mu = -\frac{2\mu\ (\eta\ +\ \nu) + \eta\,\nu + 3\,\mu^2}{(\eta+\mu)\,(\nu+\mu)}, \quad SI_{\nu_1} = -\frac{\nu_1}{\nu+\mu}, \quad SI_\eta = -\frac{\eta}{\eta+\mu}.$$

Using the values provided in Table 1, the sensitivity measures for different model parameters, determined with formula (3.1), are showed in Figure 3 and recapitulated in Table 2. Analysis of the Table 2 reveals that a 10% decrease (or increase) in the values of Λ, τ_0, and ν_2 results in a corresponding 10%, 10%, and 1.780% decrease (or increase) in R_0, respectively. On the other hand, a 10% increase in the values of μ, ν_1, and η leads to a reduction in R_0 by 10.094%, 1.756%, and 9.930%,, respectively. We have graphically represented the influence of selected vital parameters on R_0 in Figure 4.

It is important to mention that the relation between the rate at which asymptomatic infectious cases progress to the unreported symptomatic category ν_2 and R_0 is positive. This means that as the rate of progression increases, R_0 typically rises, indicating an increased risk of an epidemic. This underscores the importance of reporting symptomatic infectious individuals.

Table 2: Sensitivity index of R_0.

Parameter	Sensitivity index	Parameter	Sensitivity index
Λ	1	ν_1	−0.17561
τ_0	1	ν_2	0.17805
μ	−1.00939	η	−0.99301

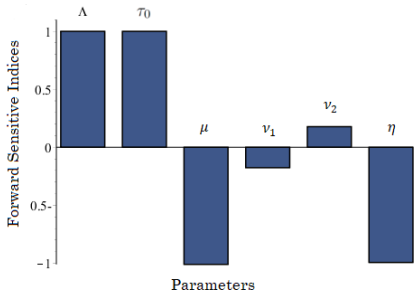

Figure 3: Forward sensitivity analysis to evaluate the impact of the parameters (2.3) on R_0.

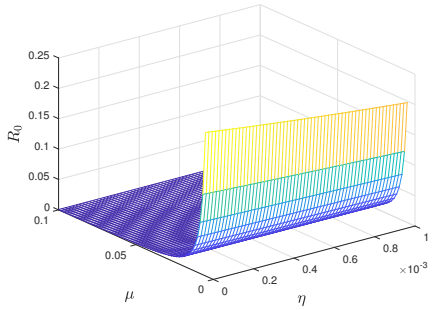

(a) R_0 versus the parameters η and μ.

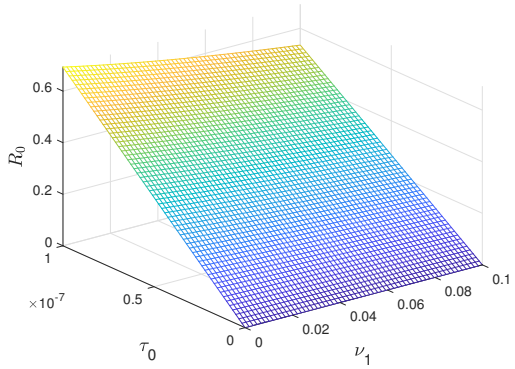

(b) R_0 versus the parameters ν_1 and τ_0.

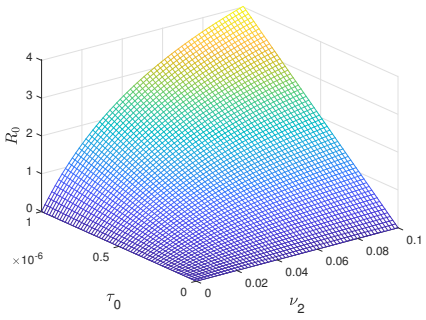

(c) R_0 versus the parameters ν_2 and τ_0.

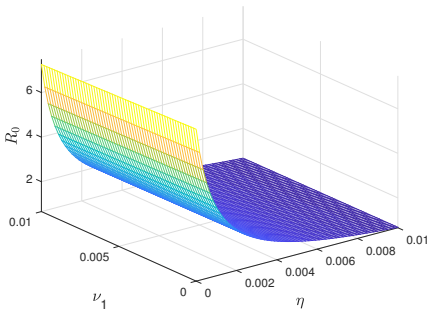

(d) R_0 versus the parameters η and ν_1.

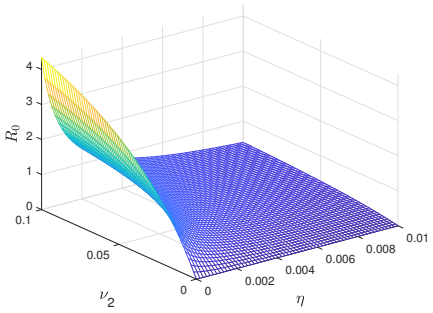

(e) R_0 versus the parameters η and ν_2.

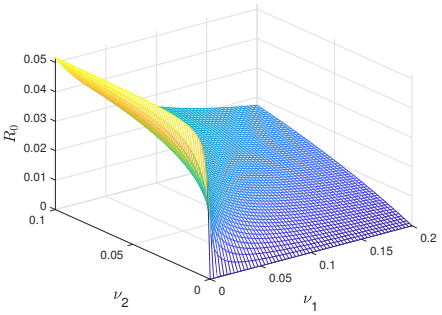

(f) R_0 versus the parameters ν_1 and ν_2.

Figure 4: Impact of of various parameters for model (2.3) on behavior of R_0.

4. Machine learning approaches for predicting the disease transmission

Machine learning approaches have been increasingly used to predict disease transmission. Although a wide range of general machine learning techniques exists, our aim is not to provide an exhaustive overview of all of them. Instead, we begin with the fundamentals of machine learning and then concentrate on physics-informed-neural-networks. The fields of statistical inference and machine learning are interconnected, with methods from one area often applied in the other and vice versa. The essential tasks of machine learning include supervised learning, unsupervised learning, reinforcement learning, and deep learning. The core principal is on training mathematical models to classify data, predict outcomes, estimate relationships, summarize data, control complex processes, and more. Any activity in this field can be viewed as a connection between models, data, algorithms, and the real world. Models are mathematical objects saved and implemented on a computer, with parameters characterizing these objects. Data refers to the collected information generated as the output of models or algorithms. Algorithms mention the process of creating models and strategies for generating output datasets. Finally, the real world, they relate to scenarios that allow the data generation, identification, and application for decision-making and control. Machine learning merges elements from both fields, combining data and algorithms. The presented Flowchart 5 outlines each step in the machine learning process. This section, aims to offer insights, analyses, and predictions using data to help guide future decisions. We begin with a brief introduction to the basics of physics-informed-neural-networks (PINNs), emphasizing the importance for our model. Next, we explore fundamental techniques and results.

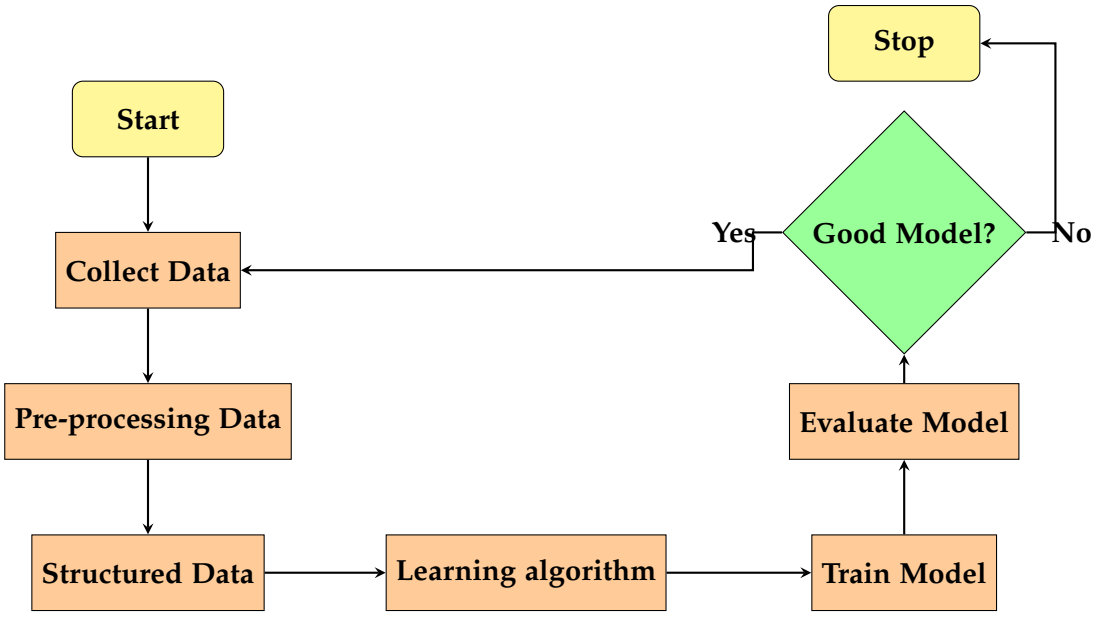

Figure 5: Diagram representing the machine learning workflow [33].

4.1. *Introduction to physics-informed-neural-networks (PINNs)*

The PINNs are a machine learning technique that merges neural networks with principles from physics to solve complex physical problems. Recently, PINNs have demonstrated exceptional results by incorporating neural networks with differential equations, while accurately fitting data. In essence, they apply neural networks to simulate nonlinear models while minimizing the essential data and limiting the model's search space applying previous knowledge and expertise. Initially, PINNs proposed by Raissi et al. [25], integrating physical information into the neural network by creating a suitable loss function, considered as an example of an inverse problem. Physics-informed neural nets for control PINC

[3] is designed for control problems. It can simulate longer-range time horizons that are not predetermined during training. This variable simulation time is achieved by incorporating inputs into the PINC network, conveying the initial condition and the control signal for a particular time interval. Simulating variable long-range intervals involves running the PINC network across a sequence of shorter intervals. The network predictions are linked in a self-feedback mode, where the initial state of the next interval is set to the last predicted state of the previous interval. To apply the PINNs method for fractional order estimation, we define the neural network as follows using a nonlinear activation function σ [12]:

$$N(X) = W_n\sigma(W_{n-1}\sigma(\cdots(W_2\sigma(W_1X + b_1) + b_2) + \cdots) + b_{n-1}) + b_n.$$

PINNs integrate PDEs and their initial and boundary conditions into the loss function of the neural network through automatic differentiation (AD) [35], this process minimizes the sum of the mean-squared PDEs-residuals and the mean-squared error (MES) in the initial or boundary conditions with respect to the neural network parameters. Typically, AD is used to optimize the weights W_i and biases b_i of the network. Consider the form of nonlinear PDEs parameterized by λ [25, 26]:

$$u_t + \mathcal{N}(u;\lambda) = 0.$$

The function $\mathcal{N}(.;\lambda)$ is a nonlinear operator, and $u(x,t)$ is the solution. When using PINNs to solve PDEs, the purpose is to find the optimal parameters λ that minimize a suitably defined loss function. To integrate the general fractional derivative defined in (2.1), we consider the general form of the equations, abbreviated as follows:

$$^{C}D^{\alpha,\beta,\gamma}_{a,t,w}u + \mathcal{N}(u;\lambda) = 0. \tag{4.1}$$

Controlled by the initial condition provided:

$$u(0) = u_0.$$

To obtain a numerical estimation of the residual, each equation is tested at selected collocation points. First, the domain $t \in [a,b]$ is discretized into n parts as $t_1 = a, t_2, \ldots, t_n = b$. Using the output of the neural network $N(\cdot)$, the loss function is then constructed as follows [30]:

$$\text{Loss} = \text{Loss}_{EQ} + \text{Loss}_{IC},$$

where

$$\text{Loss}_{EQ} = \sum_{i=1}^{n}\left[[^{C}D^{\alpha,\beta,\gamma}_{a,t,w}N]_{t=t_i} + \mathcal{N}(N(t_i);\lambda)\right], \quad \text{Loss}_{IC} = (u(0) - u_0)^2.$$

The mean squared error, which is chosen as the loss function for the neural network, is optimized using optimizers such as L-BFGS or Adam. For a more detailed explanation, refer to [23, 37]. Equation (4.1) can be transformed into the following form:

$$\mathcal{F}(u;\lambda) = 0,$$

where $\mathcal{F}$ is a differential fractional operator involving a general fractional derivative as defined in definition (2.1). In this study, we define $\lambda = [\alpha,\beta,\gamma]^T$ and $u_0 = [S_0, I_0, R_0, U_0, H_0]^T$ for estimating the fractional orders. In the next section, we apply the main steps showed in Diagram 5 to implement the PINNs approach for estimating fractional order derivatives. First step, we define the immediate problem. Next, we construct a PINNs architecture adapted to tackle the defined problem. Once the architecture is created, we train the PINNs employing appropriate data and mathematical techniques. Finally, we evaluate the performance of the trained PINNs to assess their effectiveness.

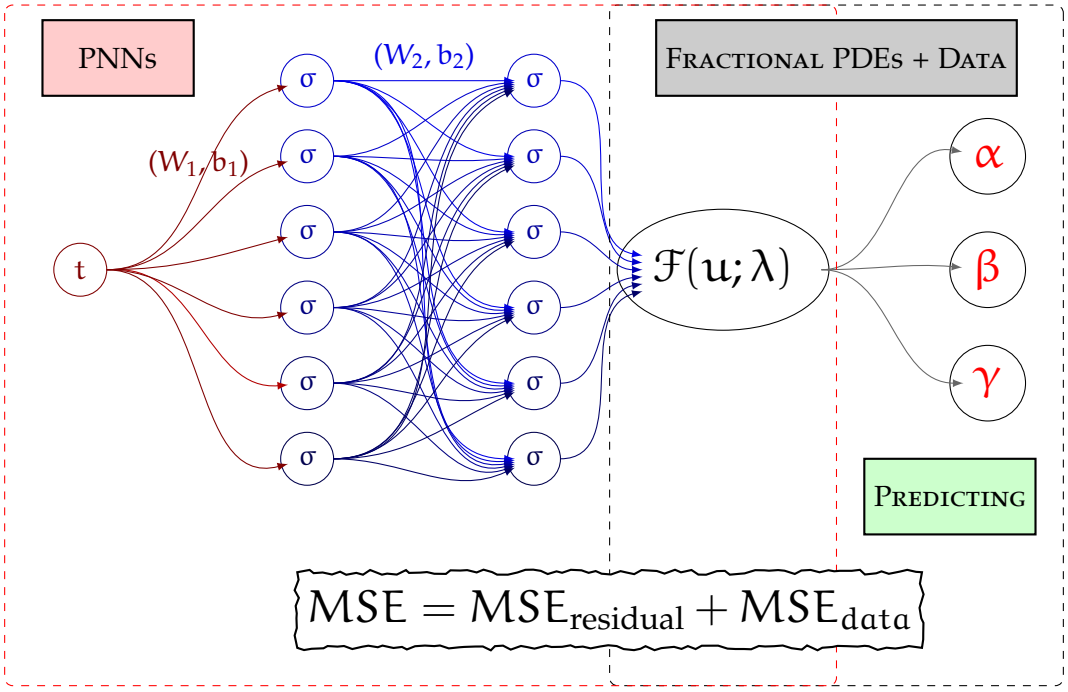

Figure 6: Illustration of the application of PINNs for solving time-fractional diffusion equations.

4.2. *Predicting a fractional derivative using the PINNs method*

Several efforts have been tried to use the PINNs for analyzing, modeling, and predicting the transmission of COVID-19 (see for example [9, 10, 21]). To use PINNs to the system (2.3), we define the residual term as follows:

$$F(t) = \begin{bmatrix} {}^{c}D^{\alpha,\beta,\gamma}_{a,t,w} S(t) - \Lambda + \tau(t)S(t)[I(t)+U(t)] + \mu S(t) \\ {}^{c}D^{\alpha,\beta,\gamma}_{a,t,w} I(t) - \tau(t)S(t)[I(t)+U(t)] + (\nu+\mu)I(t) \\ {}^{c}D^{\alpha,\beta,\gamma}_{a,t,w} R(t) - \nu_1 I(t) + (\eta+\mu)R(t) \\ {}^{c}D^{\alpha,\beta,\gamma}_{a,t,w} U(t) - \nu_2 I(t) + (\eta+\mu)U(t) \\ {}^{c}D^{\alpha,\beta,\gamma}_{a,t,w} H(t) - \eta(R(t)+U(t)) + \mu H(t) \end{bmatrix}.$$

We evaluate F at a certain number of points. The mean residual squared error of F is given by:

$$MSE_{residual} = MSE_{S_{residual}} + MSE_{I_{residual}} + MSE_{R_{residual}} + MSE_{U_{residual}} + MSE_{H_{residual}},$$

where

$$MSE_{S_{residual}} = \frac{1}{N}\sum_{i=1}^{N} \left| {}^{c}D^{\alpha,\beta,\gamma}_{a,t_i,w} S(t_i) - \Lambda + \tau S(t_i)[I(t_i)+U(t_i)] + \mu S(t_i) \right|^2,$$

$$MSE_{I_{residual}} = \frac{1}{N}\sum_{i=1}^{N} \left| {}^{c}D^{\alpha,\beta,\gamma}_{a,t_i,w} I(t_i) - \tau S(t_i)[I(t_i)+U(t_i)] + (\nu+\mu)I(t_i) \right|^2,$$

$$MSE_{R_{residual}} = \frac{1}{N}\sum_{i=1}^{N} \left| {}^{c}D^{\alpha,\beta,\gamma}_{a,t_i,w} R(t_i) - \nu_1 I(t_i) + (\eta+\mu)R(t_i) \right|^2,$$

$$MSE_{U_{residual}} = \frac{1}{N}\sum_{i=1}^{N} \left| {}^{c}D^{\alpha,\beta,\gamma}_{a,t_i,w} U(t_i) - \nu_2 I(t_i) + (\eta+\mu)U(t_i) \right|^2,$$

$$MSE_{H_{residual}} = \frac{1}{N}\sum_{i=1}^{N} \left| {}^{c}D^{\alpha,\beta,\gamma}_{a,t_i,w} H(t_i) - \eta(R(t_i)+U(t_i)) + \mu H(t_i) \right|^2.$$

The training data set typically consists of a collection of points with known values, located within the domain. The mean squared error of the data is:

$$MSE_{data} = MSE_{S_{data}} + MSE_{I_{data}} + MSE_{R_{data}} + MSE_{U_{data}} + MSE_{H_{data}},$$

where

$$MSE_{S_{data}} = \frac{1}{N}\sum_{i=1}^{N}\left|S(t_i) - S_i^0\right|^2, \quad MSE_{I_{data}} = \frac{1}{N}\sum_{i=1}^{N}\left|I(t_i) - I_i^0\right|^2, \quad MSE_{R_{data}} = \frac{1}{N}\sum_{i=1}^{N}\left|R(t_i) - R_i^0\right|^2,$$

$$MSE_{U_{data}} = \frac{1}{N}\sum_{i=1}^{N}\left|U(t_i) - U_i^0\right|^2, \quad MSE_{H_{data}} = \frac{1}{N}\sum_{i=1}^{N}\left|H(t_i) - H_i^0\right|^2.$$

Note that $S_i^0, I_i^0, R_i^0, U_i^0, H_i^0$ are the observed data at time t_i. The total loss is defined as:

$$MSE = MSE_{residual} + MSE_{data}.$$

The solution provides the optimal values of α and β that minimize the MSE for the fractional operator. Table 3 shows this optimal values of α and β after training the neural networks for 50000 epochs. The use of the PINNs method allowed for efficient estimation and fine-tuning of the fractional order parameters, resulting in $\alpha = 0.6173$ and $\beta = 0.9569$. These predicted fractional order not only offer insights into the underlying dynamics of the system but also facilitate an accurate representation of the complex behavior of the model. Using these values, one can then visualize the transmission of the model predictions compared to the solution of the system (2.2) which is plotted in Figure 8. The visualization shows how accuratly the model predictions align with the actual system's behavior, validating the effectiveness of the PINNs approach in capturing and modeling the disease transmission dynamics. This precise correlation between model predictions and real-world observations demonstrates the capacity of PINNs to improve the understanding of epidemiological systems and enhance predictive capabilities.

Table 3: Estimation of α and β.

Epoch	32000	33000	34000	35000	36000	37000	38000	39000	40000
α	0.6171	0.6172	0.6172	0.6172	0.6172	0.6173	0.6173	0.6172	0.6172
β	0.9568	0.9568	0.9568	0.9568	0.9569	0.9569	0.9569	0.9569	0.9569

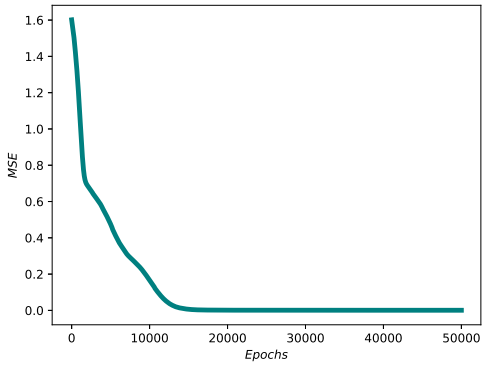

Figure 7: The loss represents the difference between the predicted and exact values.

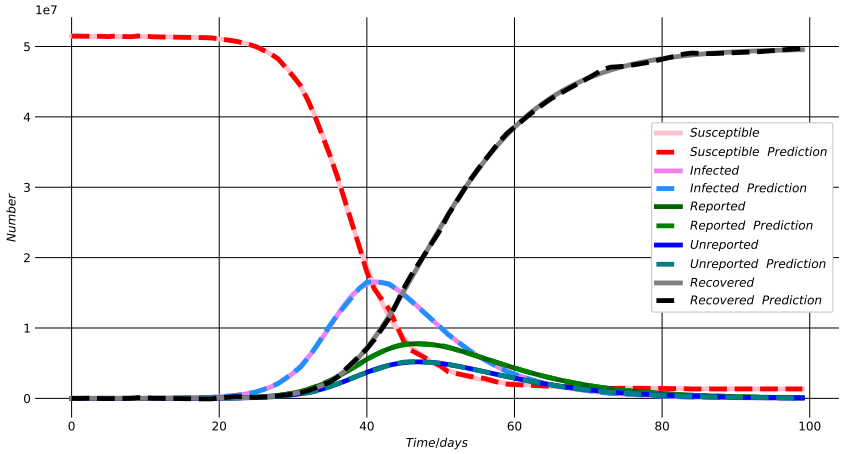

Figure 8: The compartments with predicted values of $\alpha = 0.6173$ and $\beta = 0.9569$.

5. Conclusion

In conclusion, this study supported the applicability and influence of a general fractional operator on real-world problems, specifically the COVID-19 epidemic. It emphasized the essential role of machine learning tools in estimating the parameters. The study began by presenting the existence, uniqueness, and stability analysis theorems, along with numerical simulation of the solutions of the model. It showcased the existence and boundedness of non-negative solutions and established the local stability of the equilibrium states. This paper proposed an advanced artificial intelligence technique based on PINNs to predict the fractional derivative parameters α and β derived from selected data for the compartmental model. The PINNs approach captured the complicated dynamics of the disease (COVID-19) by including a modified susceptible, asymptomatic infectious, unreported symptomatic infectious, reported symptomatic infectious, and healed (SIURH) compartmental model with artificial intelligence. We treated specifically the system (2.3) as another network to address unknown fractional derivative order. The study presents several opportunities for future research and further development. First, it suggests exploring the application of PINNs and other advanced AI methods to diseases beyond COVID-19. Second, investigating the performance of PINNs across various regional datasets and scenarios could offer insights into the adaptability and scalability of these methods. Finally, optimizing fractional PINNs and their training procedures could lead to more efficient and precise parameter estimation, providing more robust tools for decision-makers in public health and epidemiology.

Acknowledgments

The authors extend their appreciation to the Deanship of Research and Graduate Studies at King Khalid University for funding this work through Large Research Project under grant number RGP 2/174/45.

References

[1] Q. T. Ain, *Nonlinear stochastic cholera epidemic model under the influence of noise*, J. Math. Techniques Model., **1** (2024), 52–74. 1

[2] H. Aghdaoui, M. Tilioua, K. S. Nisar, I. Khan, *A Fractional Epidemic Model with Mittag-Leffler Kernel for COVID-19*, Math. Biol. Bioinform., **16** (2021), 39–56. 1

[3] E. A. Antonelo, E. Camponogara, L. O. Seman, J. P. Jordanou, E. R. de Souza, J. F. Hübner, *Physics-informed neural nets for control of dynamical systems*, Neurocomputing, **579** (2024). 4.1

[4] L. Boujallal, *Stability analysis of fractional order mathematical model of leukemia*, Int. J. Math. Model. Comput., **11** (2021), 15–27. 2.4.2

[5] E. Dahy, A. M. Elaiw, A. A. Raezah, H. Z. Zidan, A. E. A. Abdellatif, *Global Properties of Cytokine-Enhanced HIV-1 Dynamics Model with Adaptive Immunity and Distributed Delays*, Computation, **11** (2023), 1–36. 3.2

[6] O. Diekmann, J. A. P. Heesterbeek, J. A. J. Metz, *On the definition and the computation of the basic reproduction ratio R0 in models for infectious diseases in heterogeneous populations*, J. Math. Biol., **28** (1990), 365–382. 2.4.1

[7] A. Din, Y. Li, A. Yusuf, *Delayed hepatitis B epidemic model with stochastic analysis*, Chaos Solitons Fractals, **146** (2021), 16 pages. 1

[8] A. Haleem, R. Vaishya, M. Javaid, I. H. Khan, *Artificial Intelligence (AI) applications in orthopaedics: an innovative technology to embrace*, J. Clin. Orthop. Trauma, **11** (2020), S80–S81. 1

[9] S. Han, L. Stelz, H. Stoecker, L. Wang, K. Zhou, *Approaching epidemiological dynamics of COVID-19 with physics-informed neural networks*, J. Frank. Inst., **361** (2023). 4.2

[10] F. Heldmann, S. Berkhahn, M. Ehrhardt, K. Klamroth, *PINN training using biobjective optimization: the trade-off between data loss and residual loss*, J. Comput. Phys. **488** (2023), 21 pages. 4.2

[11] A. Jafarian, M. Mokhtarpour, D. Baleanu, *Artificial neural network approach for a class of fractional ordinary differential equation*, Neural Comput. Appl., **28** 2017, 765–773. 1

[12] A. D. Jagtap, K. Kawaguchi, G. E. Karniadakis, *Adaptive activation functions accelerate convergence in deep and physics-informed neural networks*, J. Comput. Phys., **404** (2020), 23 pages. 4.1

[13] P. Jiang, X. Fu, Y. Van Fan, J. J. Klemeš, P. Chen, S. Ma, W. Zhang, *Spatial-temporal potential exposure risk analytics and urban sustainability impacts related to COVID-19 mitigation: A perspective from car mobility behaviour*, J. Clean. Prod., **279** (2021), 1–15. 1

[14] H. Khalid, *A New Generalized Definition of Fractional Derivative with Non-Singular Kernel*, Computation, **8** (2020), 1–9. 2.1, 2.2, 2.1

[15] L. Li, L. Qin, Z. Xu, Y. Yin, X. Wang, B. Kong, J. Bai, Y. Lu, Z. Fang, Q. Song, K. Cao, D. Liu, G. Wang, Q. Xu, X. Fang, S. Zhang, J. Xia, J. Xia, *Artificial intelligence distinguishes COVID-19 from community acquired pneumonia on chest CT*, Radiology, (2020). 1

[16] Z. Liu, P. Magal, O. Seydi, G. Webb, *Predicting the cumulative number of cases for the COVID - 19 epidemic in China from early data*, arXiv:2002.12298v1, (2020), 1–10. 1, 2.2, 1

[17] H. Luo, Q.-L. Tang, Y.-X. Shang, S.-B. Liang, M. Yang, N. Robinson, J.-P. Liu, *Can Chinese medicine be used for prevention of corona virus disease 2019 (COVID-19)? A review of historical classics, research evidence and current prevention programs*, Chin. J. Integr. Med., **26** 2020, 243–250. 1

[18] P. Magal, G. Webb, *Predicting the number of reported and unreported cases for the COVID - 19 epidemic in South Korea, Italy, France and Germany*, MedRxiv, (2020), 1–16. 1, 2.2, 1

[19] S. Marino, I. B. Hogue, C. J. Ray, D. E. Kirschner, *A methodology for performing global uncertainty and sensitivity analysis in systems biology*, J. Theoret. Biol., **254** (2008), 178–196. 3.2

[20] X. Ning, J. Guan, X.-A. Li, Y. Wei, F. Chen, *Physics-informed neural networks integrating compartmental model for analyzing COVID-19 transmission dynamics*, Viruses, **15** (2023), 1–16. 1

[21] X. Ning, L. Jia, Y. Wei, X.-A. Li, F. Chen, *Epi-DNNs: Epidemiological priors informed deep neural networks for modeling COVID-19 dynamics*, Comput. Biol. Med., **158** (2023), 1–9. 4.2

[22] M. Pakdaman, A. Ahmadian, S. Effati, S. Salahshour, D. Baleanu, *Solving differential equations of fractional order using an optimization technique based on training artificial neural network*, Appl. Math. Comput., **293** (2017), 81–95. 1

[23] G. Pang, L. Lu, G. E. Karniadakis, *fPINNs: fractional physics-informed neural networks*, SIAM J. Sci. Comput., **41** (2019), A2603–A2626. 1, 4.1

[24] B. Rahnsch, L. Taghizadeh, *Network-based uncertainty quantification for mathematical models in epidemiology*, J. Theoret. Biol., **577** (2024), 12 pages 1

[25] M. Raissi, P. Perdikaris, G. E. Karniadakis, *Physics informed deep learning (part i): Data-driven solutions of nonlinear partial differential equations*, arXiv preprint arXiv:1711.10561, (2017). 4.1

[26] M. Raissi, P. Perdikaris, G. E. Karniadakis, *Physics-informed neural networks: A deep learning framework for solving forward and inverse problems involving nonlinear partial differential equations*, J. Comput. Phys., **378** (2019), 686–707. 4.1

[27] F. Rostami, A. Jafarian, *A new artificial neural network structure for solving high-order linear fractional differential equations*, Int. J. Comput. Math., **95** (2018), 528–539. 1

[28] S. M. A. Shah, H. Tahir, A. Khan, W. A. Khan, A. Arshad, *Stochastic Model on the Transmission of Worms in Wireless Sensor Network*, J. Math. Techniques Model., **1** (2024), 75–88.

[29] S. M. Sivalingam, P. Kumar, V. Govindaraj, *The hybrid average subtraction and standard deviation based optimizer*, Adv. Eng. Softw., **176** (2023). 1

[30] S. M. Sivalingam, P. Kumar, V. Govindaraj, *A neural networks-based numerical method for the generalized Caputo-type fractional differential equations*, Math. Comput. Simulation, **213** (2023), 302–323. 1, 4.1

[31] C. Sohrabi, Z. Alsafi, N. O'Neill, M. Khan, A. Kerwan, A. Al-Jabir, C. Iosifidis, R. Agha, *World Health Organization declares global emergency: A review of the 2019 novel coronavirus (COVID-19)*, Int. J. Surg., **76** (2020), 71–76. 1

[32] M. Toufik, A. Atangana, *New numerical approximation of fractional derivative with non-local and non-singular kernel: application to chaotic models*, Eur. Phys. J. Plus, **132** (2017), 1–16. 3.1

[33] R. Verma, S. K. Gawre, N. P. Patidar, S. Nandanwar, *A state of art review on the opportunities in automatic generation control of hybrid power system*, Electric Power Systems Research, **226** (2024), 1–17. 5
[34] M. Wu, J. Zhang, Z. Huang, X. Li, Y. Dong, *Numerical solutions of wavelet neural networks for fractional differential equations*, Math. Methods Appl. Sci., **46** (2023), 3031–3044. 1
[35] C. Yang, Y. Deng, J. Yao, Y. Tu, H. Li, L. Zhang, *Fuzzing automatic differentiation in deep-learning libraries*, In: 2023 IEEE/ACM 45th International Conference on Software Engineering (ICSE), IEEE, (2023), 1174–1186. 4.1
[36] D. Zhang, L. Lu, L. Guo, G. E. Karniadakis, *Quantifying total uncertainty in physics-informed neural networks for solving forward and inverse stochastic problems*, J. Comput. Phys., **397** (2019), 19 pages. 1
[37] J. Zhang, Y. Zhao, Y. Tang, *Adaptive loss weighting auxiliary output fPINNs for solving fractional partial integro-differential equations*, Phys. D, **460** (2024), 13 pages. 1, 4.1